The impact of tetrahedral capping groups and device processing conditions on the crystal packing, thin film features and OFET hole mobility of 7,14-bis(ethynyl)dibenzo[b,def]chrysenes

Electronic Supporting Information (ESI)

Ying Shu,[a] Gavin E. Collis,*[a] Christopher Dunn,[a] Peter Kemppinen,[a] Kevin N. Winzenberg,[a] Rachel M. Williamson,[b] Ante Bilic,[a] Th. Birendra Singh,[a] Mark Bown,[a] Christopher R. McNeill[c] and Lars Thomsen[b]

Dr Ying Shu, Dr G. E. Collis, Dr Christopher Dunn, Peter Kemppinen, Dr Kevin N. Winzenberg, Dr Ante Bilic, Dr Th. Birendra Singh, Dr Mark Bown,
CSIRO Materials Science and Engineering,
Flexible Electronics Theme, Future Manufacturing Flagship,
Clayton South, Melbourne, 3169, Victoria, (Australia)
E-mail: Gavin.Collis@csiro.au

Dr Rachel M. Williamson, Dr Lars Thomsen
Australian Synchrotron
800 Blackburn Road, Clayton, VIC 3168 (Australia)

Dr Christopher R. McNeill
Department of Materials Engineering
Monash University
Melbourne, VIC 3800 (Australia)

Table of Contents

1. Differential Scanning Calorimetry (DSC)

Fig. S1. DSC curve for *t*Bu-DBC **2a**
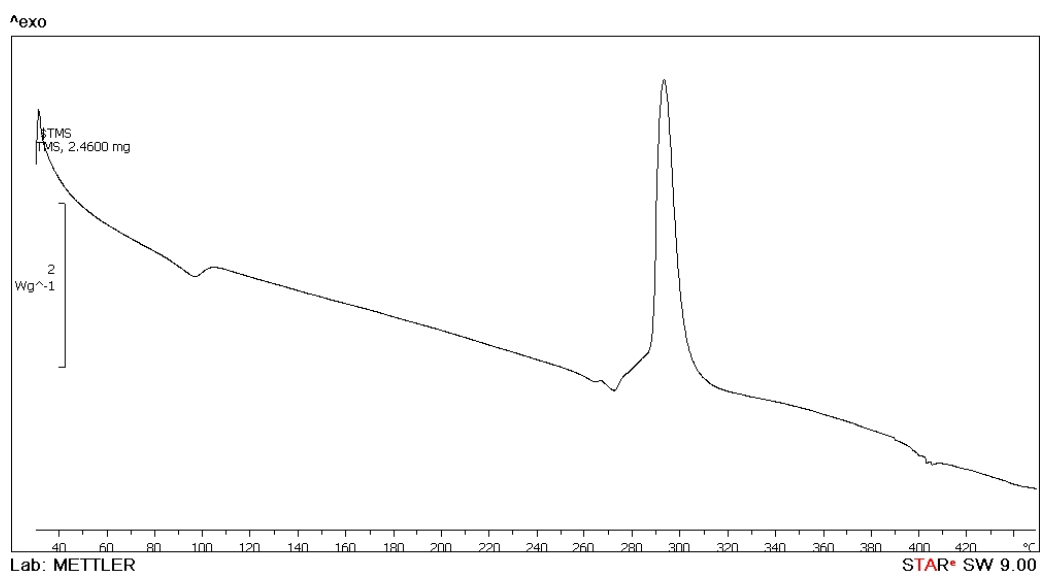
Fig. S2. DSC curve for TMS-DBC **2b**

^exo

!$YSTES2CC
YSTES2CC, 8.6500 mg

2
Wg^-1

40 60 80 100 120 140 160 180 200 220 240 260 280 300 320 340 360 380 °C

Lab: METTLER

STARe SW 9.00
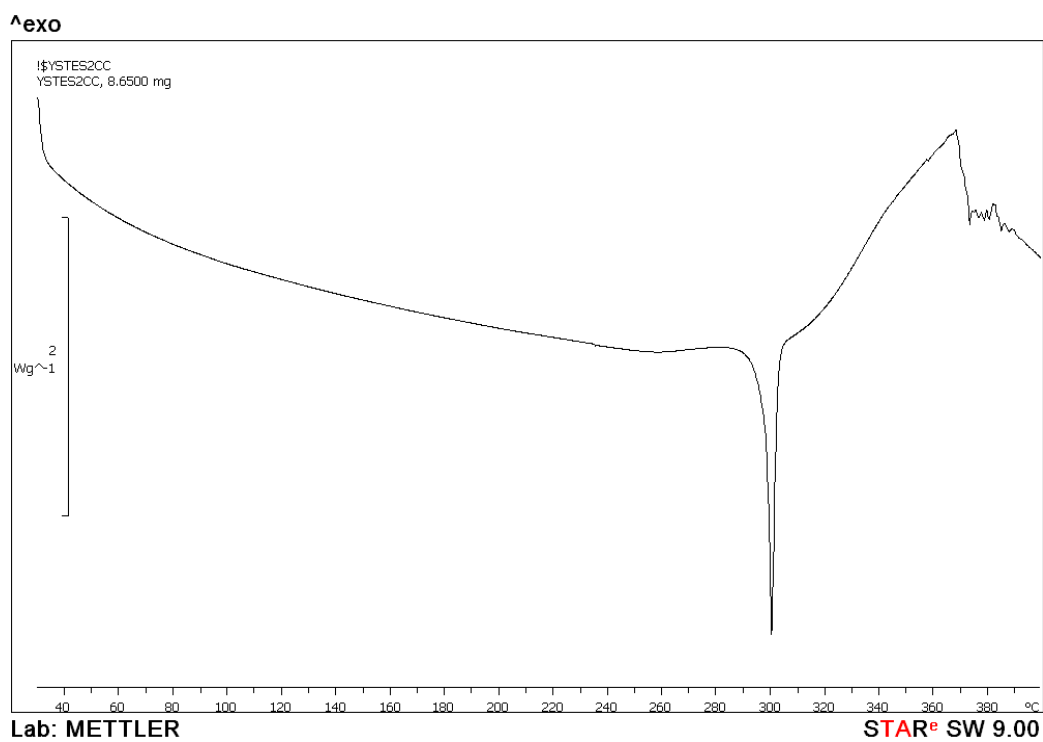
Fig. S3. DSC curve for TES-DBC **2c**

^exo

!$YSTBDMS04
YSTBDMS04, 1.5400 mg

5
Wg^-1

40 60 80 100 120 140 160 180 200 220 240 260 280 300 320 340 360 380 °C

Lab: METTLER

STARe SW 9.00
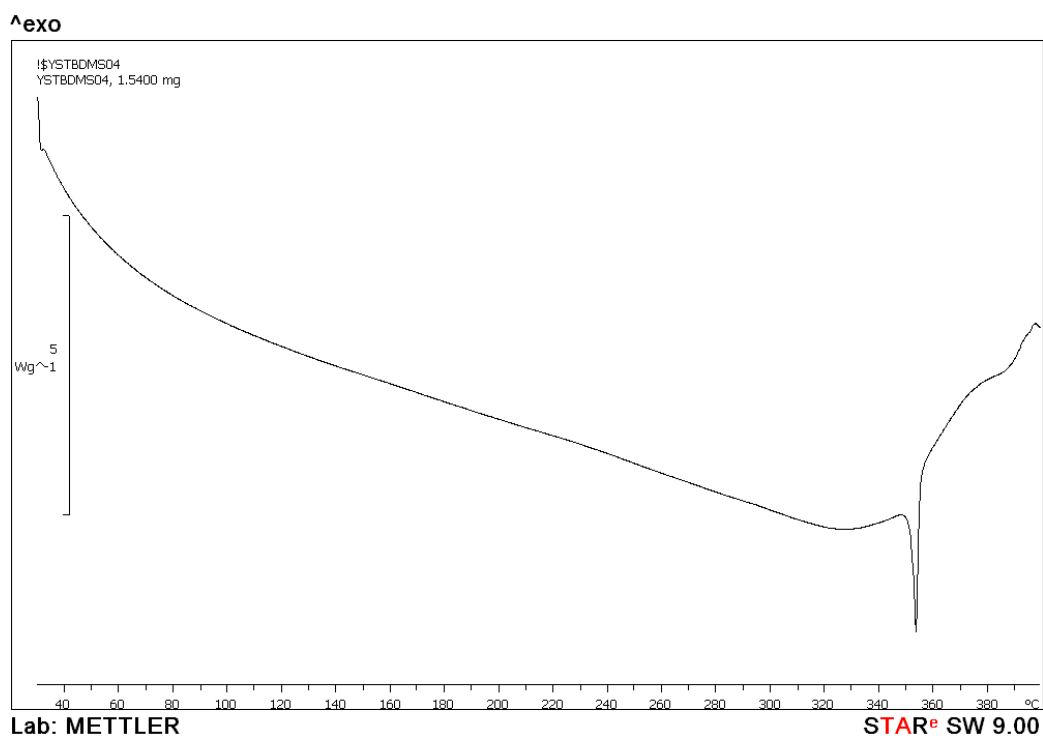
Fig. S4. DSC curve for TBDMS-DBC **2d**

^exo

!$YSTIPSCC
YSTIPSCC, 8.5200 mg

2
Wg^-1

40 60 80 100 120 140 160 180 200 220 240 260 280 300 320 340 360 380 °C

Lab: METTLER   STAR^e SW 9.00
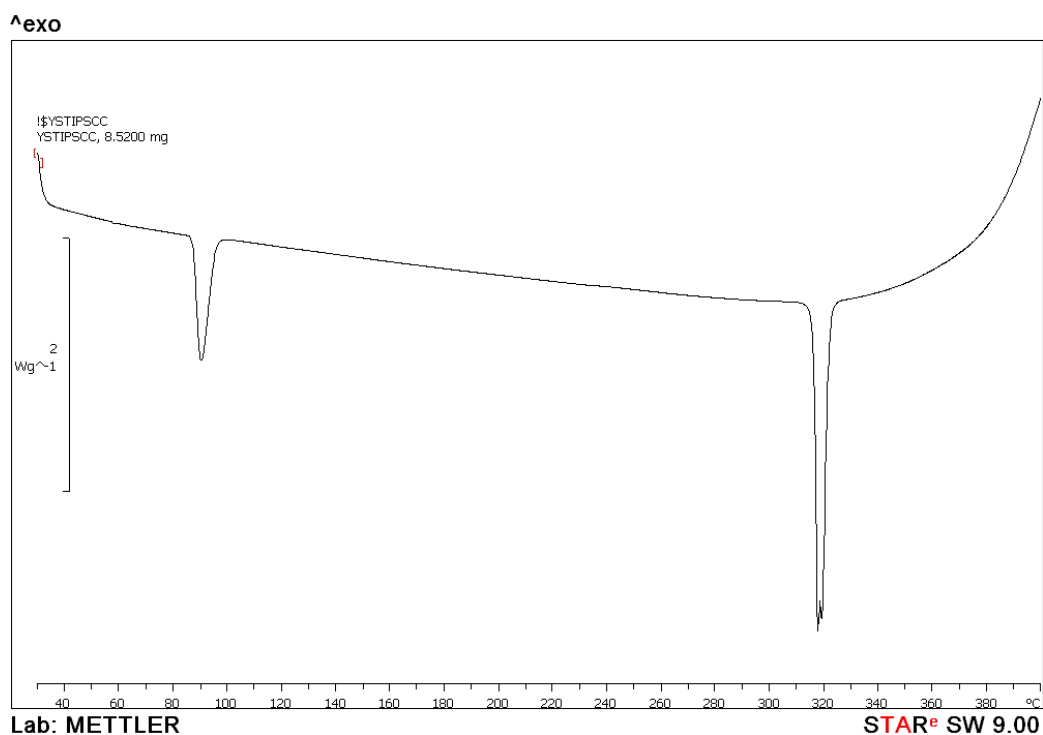
Fig. S5. DSC curve for TIPS-DBC **2e**

^exo

5
Wg^-1 !$YSTTMSS05
YSTTMSS05, 1.7400 mg

40 60 80 100 120 140 160 180 200 220 240 260 280 300 320 340 360 380 °C

Lab: METTLER   STAR^e SW 9.00
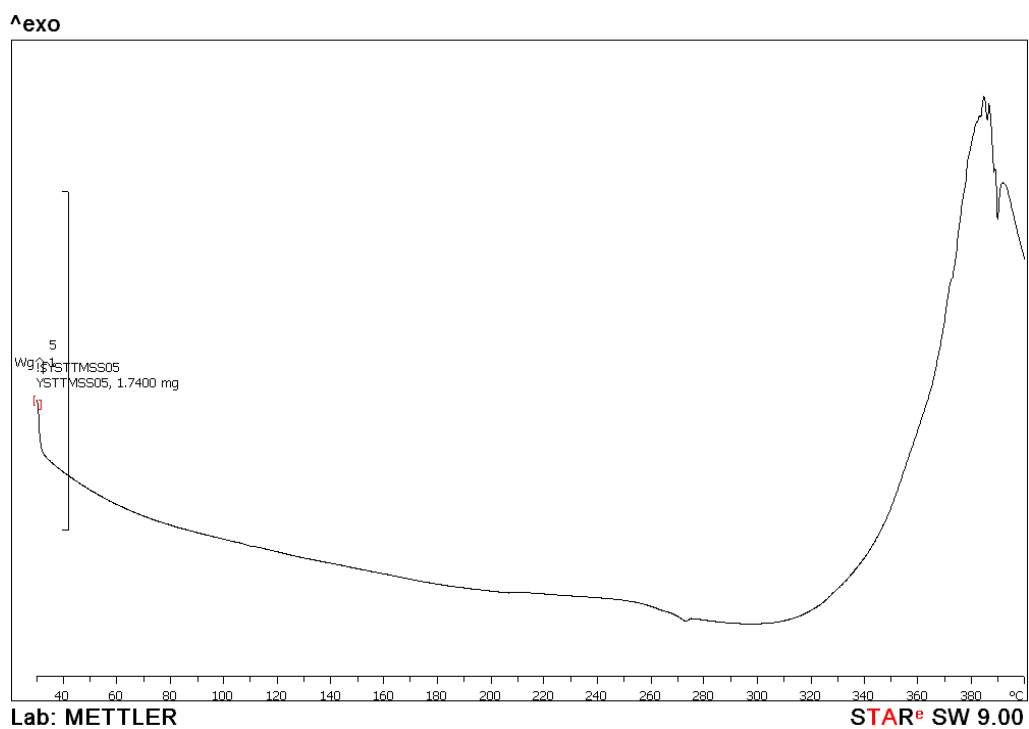
Fig. S6. DSC curve for TTMSS-DBC **2f**

2.   Solution UV/Vis spectroscopy data for DBC derivatives 2a-f.

The spectra are shown in **Fig. S7** and the absorption wavelength and molar extinction coefficient are presented in the **Table S1** below.
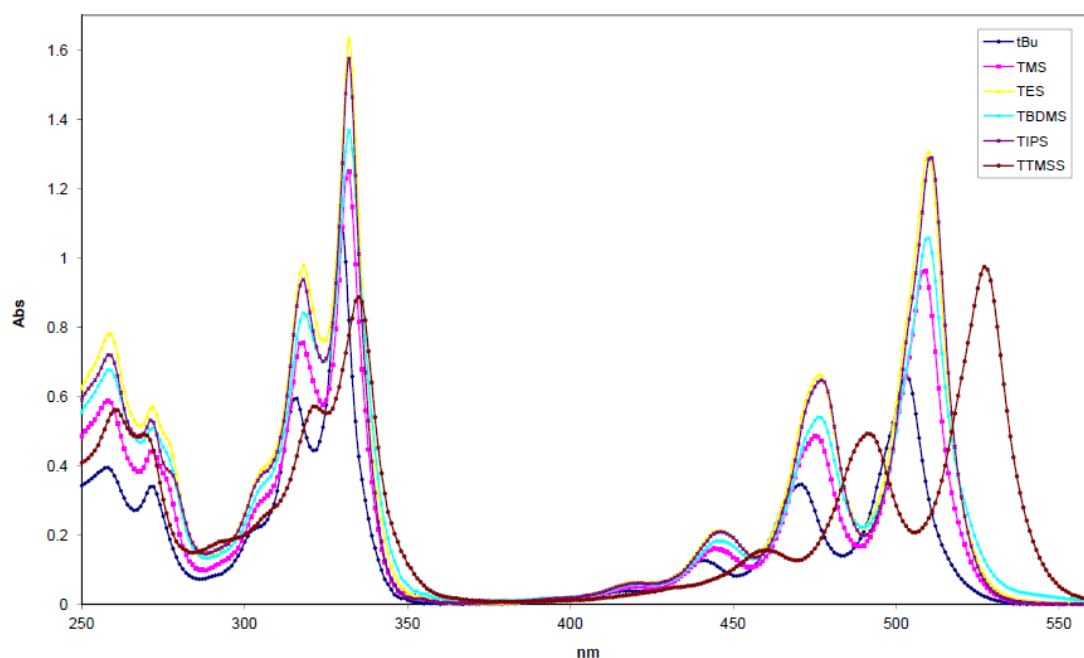

Fig. S7. UV/Visible spectra of DBC derivatives **2a-f** at 0.025 mM in dichloromethane.

3.   Cyclic Voltammetry data for DBC derivatives 2a-f.

Compound	λ_{max} onset (nm)[a]	Log ε (M^{-1}cm^{-1})	λ_{onset} (nm)	Optical bandgap (eV)[b]	Oxidation (mV)[c]	HOMO (eV)[d]	LUMO (ev)[e]
tBu-DBC **2a**	503	4.42	519	2.39	0.46	-5.26	-2.87
TMS-DBC **2b**	509	4.58	521	2.38	0.54	-5.34	-2.96
TES-DBC **2c**	510	4.72	522	2.38	0.55	-5.35	-2.97
TBDMS-DBC **2d**	510	4.63	527	2.35	0.58	-5.38	-3.03
TIPS-DBC **2e**	511	4.71	522	2.38	0.55	-5.35	-2.97
TTMSS-DBC **2f**	527	4.59	543	2.28	0.54	-5.34	-3.06

Table S1. Optical and electrochemical data for DBC derivatives **2a-f**.
[a]Measured in dichloromethane solution (0.025 mM).
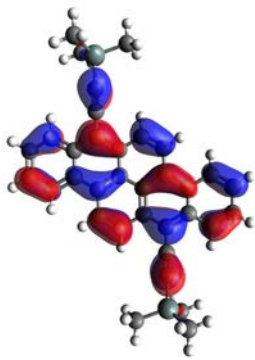[b] Determined from solution UV-visible onset
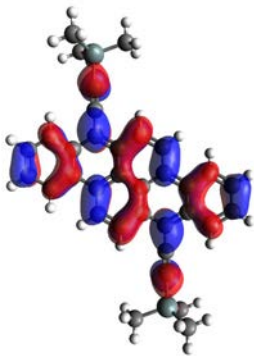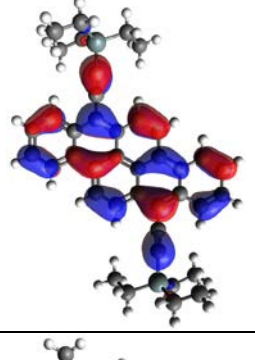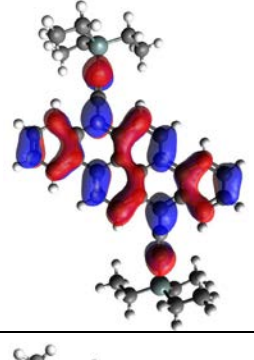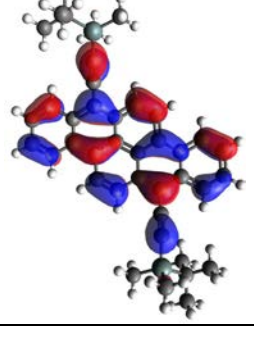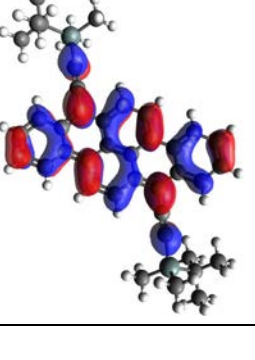[c] Cyclic voltammograms measured in dichloromethane, 1 mM, Bu$_4$NPF$_6$ (0.1 M), ambient temperature, scan rate = 100 mV s^{-1}, versus Fc/Fc$^+$ as an internal standard.
[d] Determined from E_{HOMO} = -(E_{ox} + 4.80) (eV)
[e] Energy gap (E_g) = LUMO - HOMO.

6

4.   Computational analysis

Quantum chemistry calculations have been carried using density functional theory (DFT) as implemented in Gaussian 09 suite of programs.[1] The B3LYP exchange-correlation functional[2] was used in most computations. The geometry of the gas phase DBC compounds was optimized at the B3LYP/6-31+G(d) spin-restricted level of theory. Vibrational frequency calculations were performed to verify that all the optimized geometries correspond to minima on the potential energy surfaces. Single point energy calculations were then conducted employing the optimized geometries and a larger 6-311+G(d,p) basis set. The calculated frontier molecular orbitals (MOs) densities, highest occupied (HOMO) and lowest unoccupied (LUMO) are shown in the Table below.

Compound	HOMO	LUMO
TMS-DBC **2b**		
TES-DBC **2c**		
TBDMS-DBC **2d**		

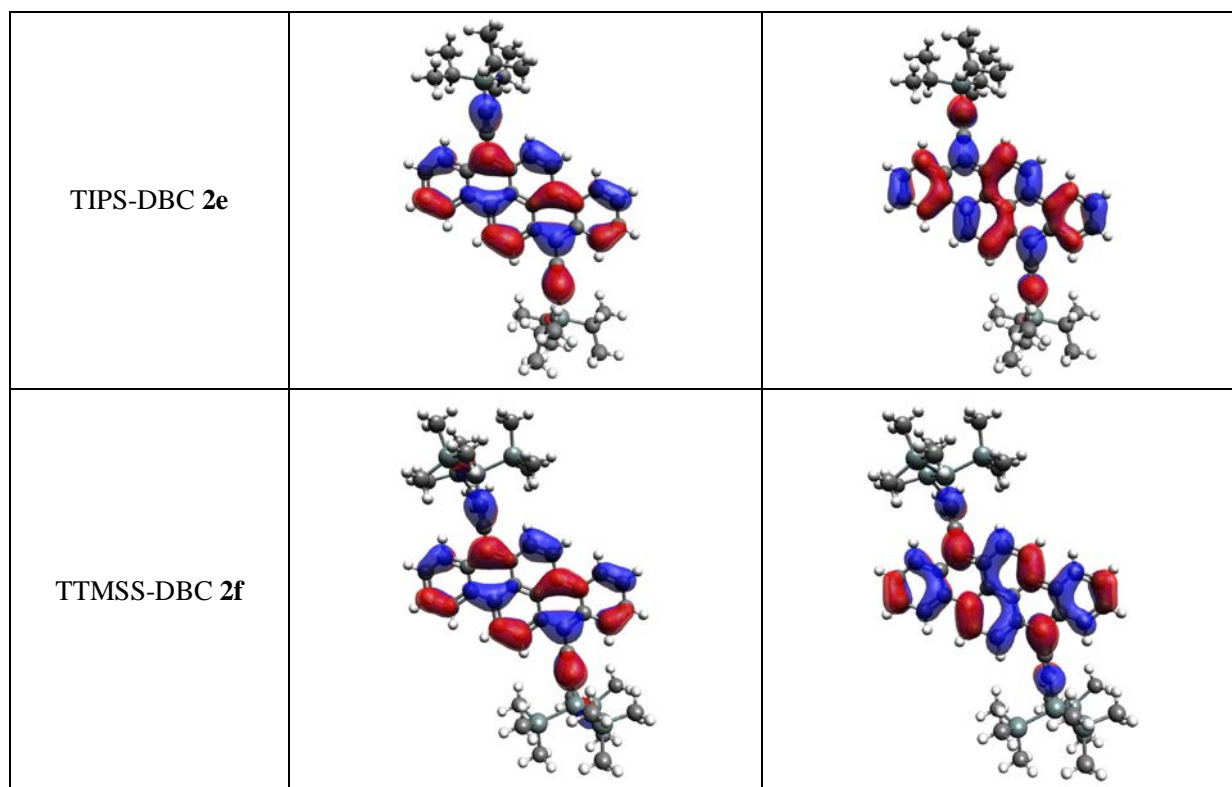|		
TIPS-DBC **2e**		
TTMSS-DBC **2f**		

Table S2: Computational HOMO and LUMO orbital images for DBC derivatives **2a-f**.

5.   Crystallographic information for TMS-DBC 2b.

CCDC 890408 contains the supplementary crystallographic data for this paper. This data can be obtained free of charge from the Cambridge Crystallographic Data Centre via www.ccdc.cam.ac.uk/data_request/cif.

TMS-DBC **2b** was grown by slow diffusion of methanol into toluene.

TMS-DBC **2b**
Red needles
$C_{33}H_{30}Si_2$
M_r 494.76
Triclinic, P-1
$a = 6.4060(13)$ Å
$b = 8.8220(18)$ Å
$c = 12.725(3)$ Å
$\alpha = 72.82(3)°$
$\beta = 76.85(3)°$
$\gamma = 83.84(3)°$
$V = 668.4\ (2)$ Å^3
$Z = 1$
$D_c = 1.229$ g cm^{-3}
$R_1 = 0.0848$
$wR2 = 0.2255$

Table S3. Crystallographic data for TMS-DBC **2b**.

6.   OFET device fabrication and testing.

Discrete Bottom Gate – Top Contact transistors (BG/TC) were fabricated on a *n*-doped (N ~ 3×10^{17} cm^{-3}) silicon wafer on which a thermally grown SiO$_2$ layer (230 nm) acts as the gate dielectric. Substrates were first cleaned with acetone, 2-propanol and then UV ozone treated. In one set of samples, the organic layer was deposited directly onto this freshly cleaned surface. In a second set, this surface was passivated using hexamethyldisilazane (HMDS): neat HMDS was dropped onto the substrate, left for 1 min and then removed by spincoating (4000 rpm for 40 s). These samples were then placed on a hotplate at 115 ºC for 20 min. In a third set, an octadecyltrichlorosilane (ODTS) surface treatment was applied by soaking freshly cleaned substrates in a 2 mM solution of octadecyltrichlorosilane in anhydrous cyclohexane for 16 hrs in a dessicator and then drying in a stream of nitrogen. All cleaning and treatments were carried out in air. After substrate cleaning and surface treatment, all samples for AFM, XRD, NEXAFS and OFET were prepared in a glovebox under an inert atmosphere. A layer of the active organic layer was deposited by thermal evaporation using an Evovac-800 system (Angstrom Engineering). Materials were deposited at a rate of 0.03 nm/s and film thickness and surface roughness were measured using the Dektak profilometer and atomic force microscopy (AFM). DBC derivatives were deposited on substrates held at temperatures of 25 and 55°C. Examples of each organic material on the three different surfaces were then built up into Top Contact OFETs by deposition of parallel Source-Drain gold electrodes by thermal evaporation through a shadow mask. OFET test was performed under an inert atmosphere (N$_2$) in a glovebox using an Agilent Technologies B1500A Semiconductor parameter analyser. The carrier mobility values presented in this work were generally averaged from measurements done on several devices. From the respective slopes, $\delta\sqrt{I_D}/\delta V_G$, device parameters: *L=60 µm, W=2000 µm (W/L = 33)*, capacitance per unit area, C_i of 10 nF/cm^2, the saturated field effect hole mobility; µ$_{hole}$, was calculated using:

$$\mu_{hole} = \frac{2L}{WC_i}(\frac{\delta\sqrt{I_D}}{\delta V_G})^2$$

Deposition of DBC **2a-f** derivatives onto SiO_2, SiO_2-HMDS and SiO_2-ODTS substrates (T_{sub} 25°C) to give BG/TC OFET devices.

	*t*Bu-DBC **2a**	TMS-DBC **2b**	TES-DBC **2c**	TBDMS-DBC **2d**	TIPS-DBC **2e**	TTMSS-DBC **2f**
SiO_2						
μ_{hole} (cm^2/Vs)	4.2×10^{-5}	4.4×10^{-5}	5.0×10^{-5}	2.9×10^{-9}	2.0×10^{-6}	0
log (I_{on}/I_{off})	1.4	1.8	1.6	1.2	0.8	0
SiO_2-HMDS						
μ_{hole} (cm^2/Vs)	1.0×10^{-5}	3.9×10^{-4}	1.1×10^{-3}	1.4×10^{-5}	7.0×10^{-5}	0
log (I_{on}/I_{off})	1.9	2.3	2.8	2.3	2.5	0
SiO_2-OTS						
μ_{hole} (cm^2/Vs)	0	1.2×10^{-2}	3.9×10^{-3}	8.3×10^{-4}	6.0×10^{-4}	4.0×10^{-5}
log (I_{on}/I_{off})	0	4.1	3.3	5.3	2.2	1.9

Table S4. OFET mobility and on/off ratios for DBC derivatives deposited on different substrate surfaces at 25°C. DBCs are deposited at a rate of 0.03 nm/s and a film thickness ~ 60 nm.

Deposition of DBC **2a-f** derivatives onto SiO_2, SiO_2-HMDS and SiO_2-ODTS substrates (T_{sub} 55°C) to give BG/TC OFET devices.

	Bu^t-DBC **2a**	TMS-DBC **2b**	TES-DBC **2c**	TBDMS-DBC **2d**	TIPS-DBC **2e**	TTMSS-DBC **2f**
SiO_2						
μ_{hole} (cm^2/Vs)	1.0×10^{-5}	1.7×10^{-4}	2.6×10^{-4}	4.0×10^{-6}	1.8×10^{-4}	0
log (I_{on}/I_{off})	1.4	4.2	2.4	1.4	1.8	0
SiO_2-HMDS						
μ_{hole} (cm^2/Vs)	2.1×10^{-5}	1.6×10^{-3}	1.3×10^{-3}	2.6×10^{-4}	2.7×10^{-4}	0
log (I_{on}/I_{off})	2.5	2.6	3.1	2.4	2.6	0
SiO_2-ODTS						
μ_{hole} (cm^2/Vs)	2.0×10^{-2}	3.3×10^{-1}	6.7×10^{-3}	2.8×10^{-3}	1.9×10^{-3}	1.5×10^{-3}
log (I_{on}/I_{off})	3.7	5.4	4.0	2.8	3.6	2.0

Table S5. OFET mobility and on/off ratios for DBC derivatives deposited on different substrate surfaces at 55°C. DBCs are deposited at a rate of 0.03 nm/s and a film thickness ~ 60 nm.

7. Near Edge X-ray Absorption Fine Structure (NEXAFS) Spectroscopy.

Carbon K-edge NEXAFS spectroscopy was performed in an ultra high vacuum (UHV) endstation chamber attached to the Soft X-ray Spectroscopy Beamline at the Australian Synchrotron. The UHV chamber which has a base pressure lower than 2×10^{-10} mbar is equipped with a SPECS Phoibos 150 hemispherical electron energy analyser. This analyser allows for the detection of carbon K-edge photoelectrons in auger electron yield (AEY) mode by setting its kinetic energy to 230eV. NEXAFS spectra were recorded at angles of 20°, 40°, 55°, 70°, and 90°, measured between the direction vector of the incident light and the surface plane of the sample. All spectra acquired were normalised following the procedures described by previous studies on dibenzochrysenes.[3] To avoid the effects of synchrotron radiation beam damage on the thin films, a sequence of scans was measured on the same spot for a significant length of time until significant changes were observed in the C K-edge spectra. The scan time was subsequently restricted to an appropriate interval in which beam damage during a single scan was negligible. Furthermore, between each angle change the beam was moved to a fresh sample area before data collection. Examples of the set of normalized NEXAFS spectra is shown below for DBC derivatives **2a-f** on SiO_2-OTDS at T_{sub} 25°C and **2b** and **2e** on SiO_2-OTDS at T_{sub} 55°C, as representative figures for the data used to calculate the tilt angles in the manuscript.
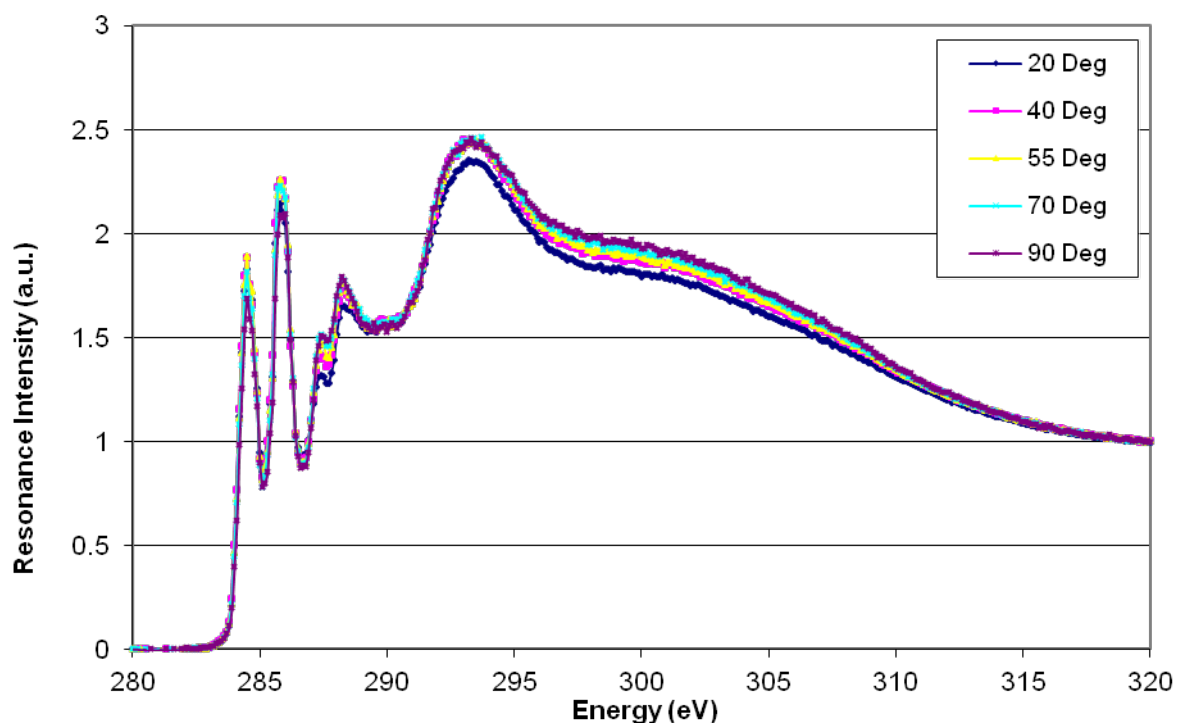
Fig. S8. Angle-resolved NEXAFS spectra for *t*Bu-DBC **2a** at T_{sub} 25°C on SiO_2-ODTS surface.
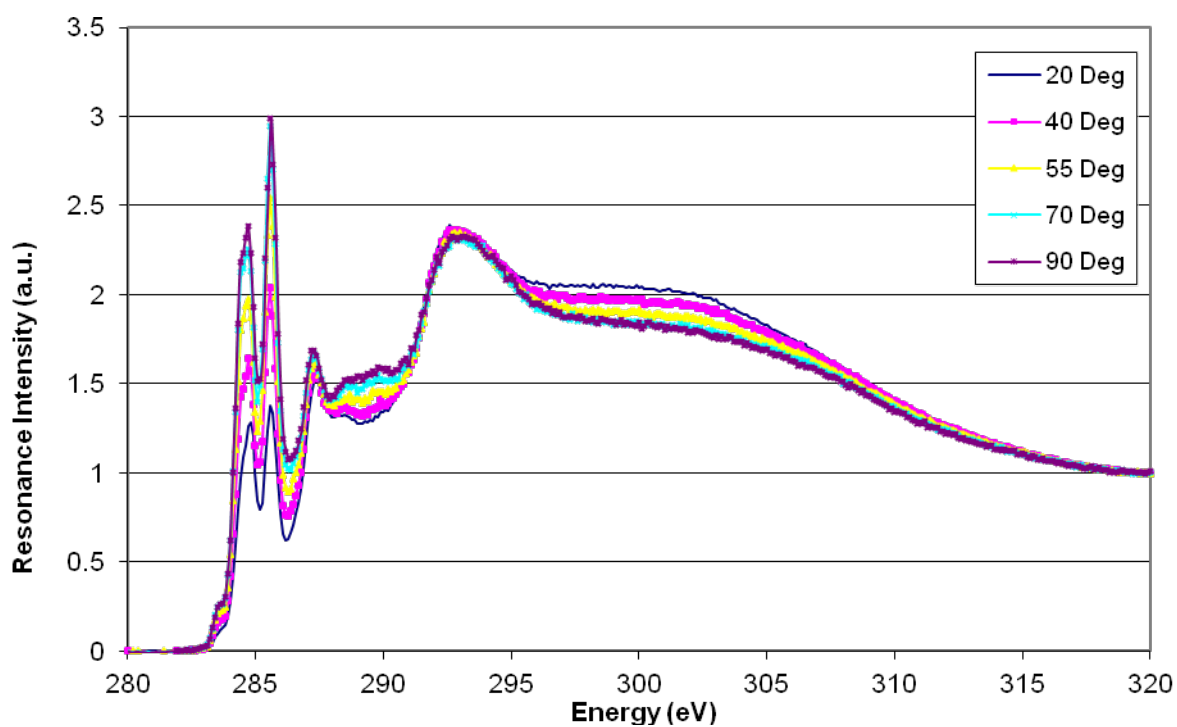

Fig. S9. Angle-resolved NEXAFS spectra for TMS-DBC **2b** at T_{sub} 25°C on SiO_2-ODTS surface.
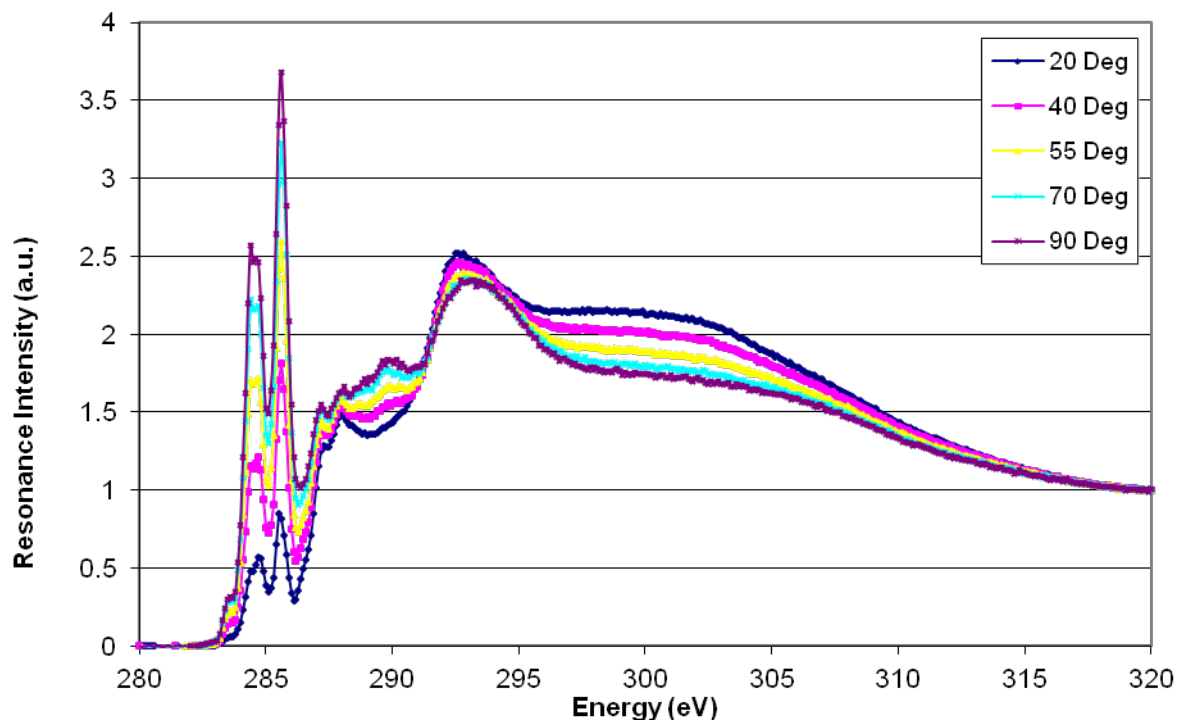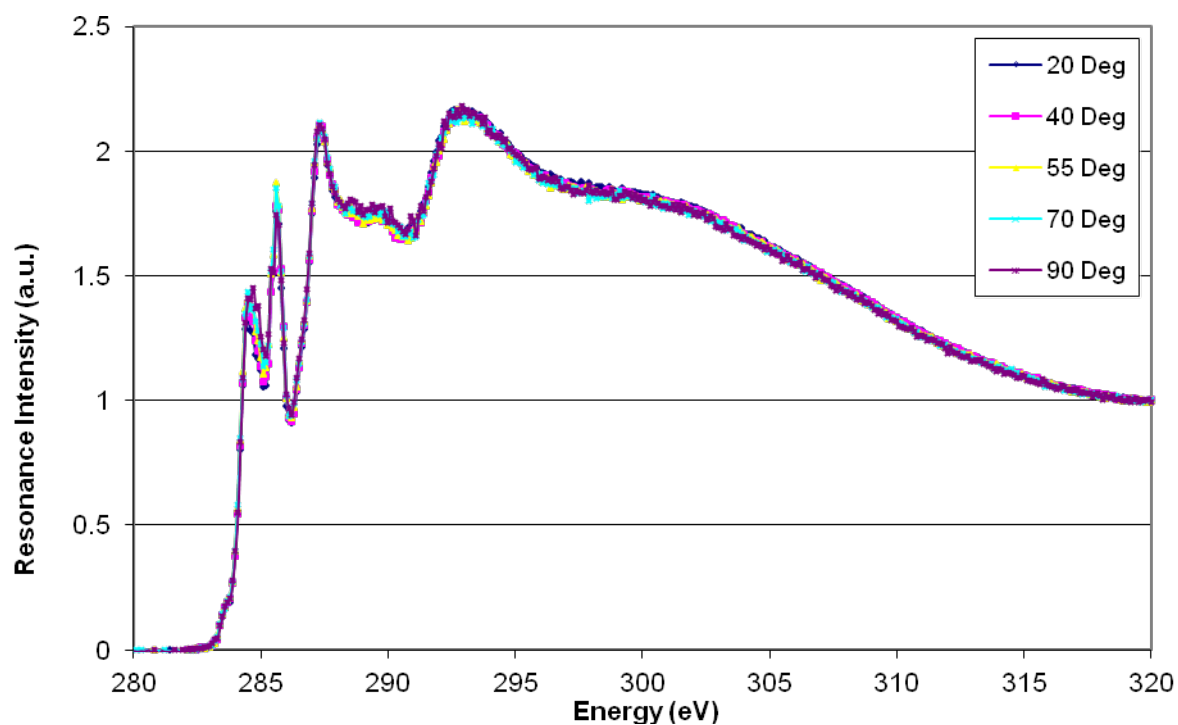
Fig. S10. Angle-resolved NEXAFS spectra for TES-DBC **2c** at T_{sub} 25°C on SiO$_2$-ODTS surface.

Fig. S11. Angle-resolved NEXAFS spectra for TBDMS-DBC **2d** at T_{sub} 25°C on SiO$_2$-ODTS surface.
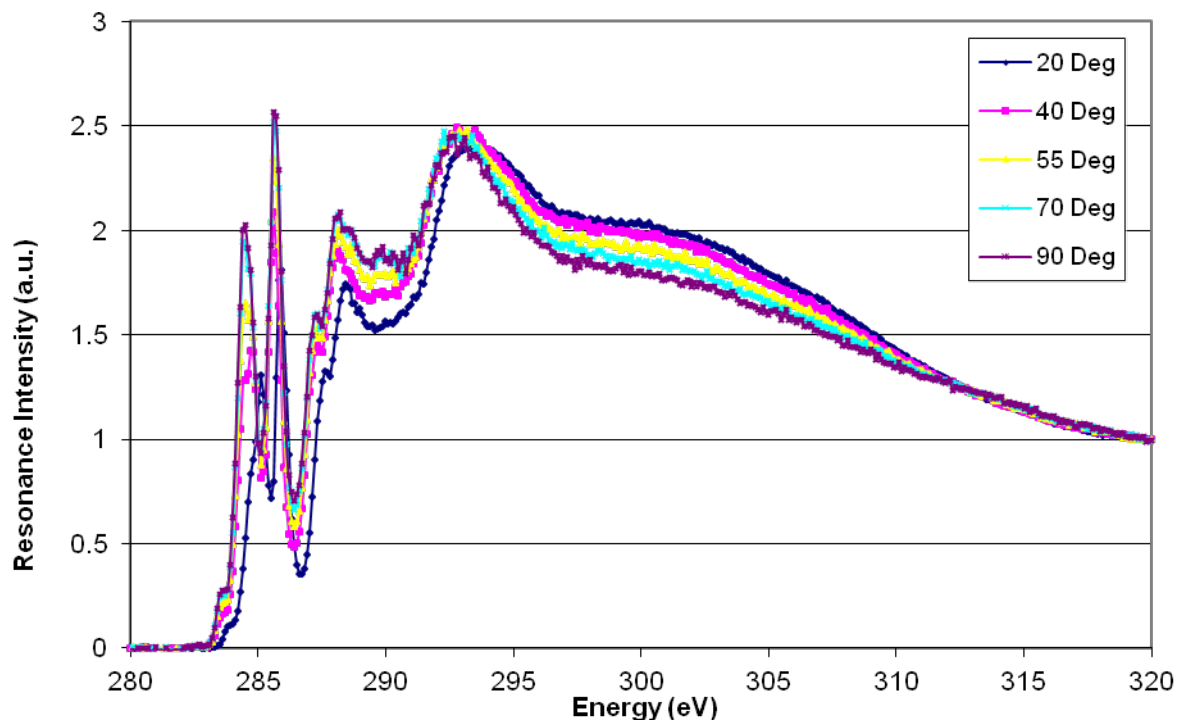
14

Fig. S12. Angle-resolved NEXAFS spectra for TIPS-DBC **2e** at T_{sub} 25°C on SiO_2-ODTS surface.
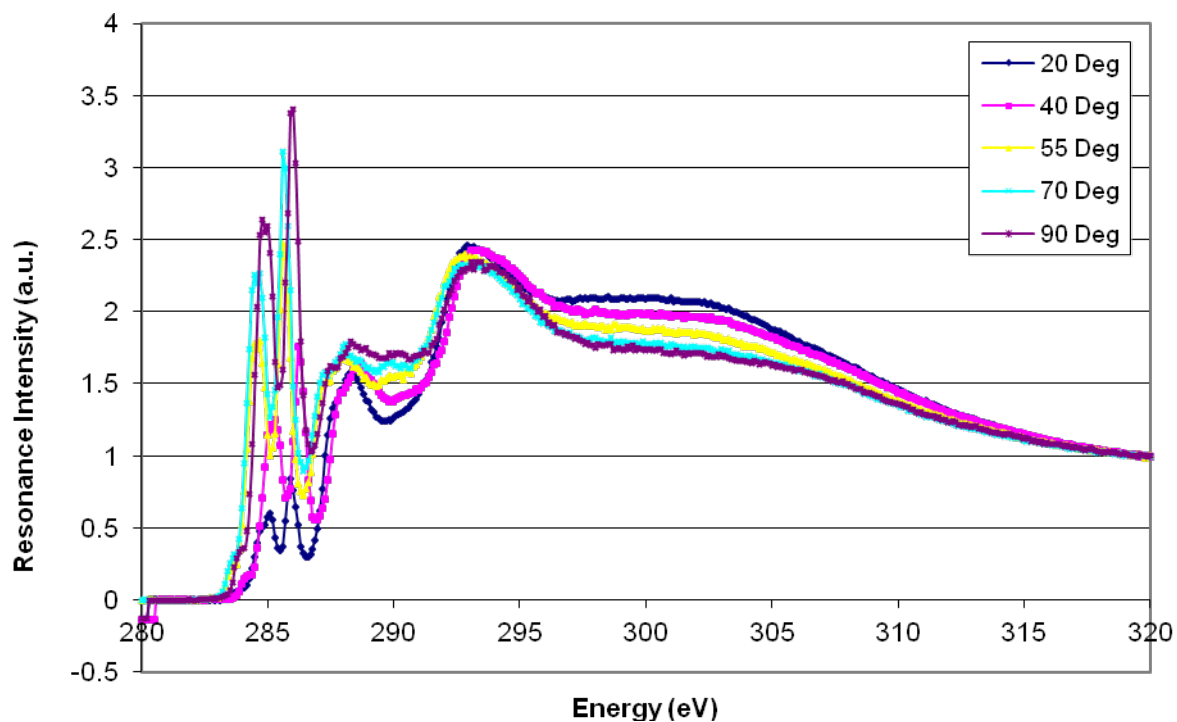

Fig. S13. Angle-resolved NEXAFS spectra for TTMSS-DBC **2f** at T_{sub} 25°C on SiO_2-ODTS surface.
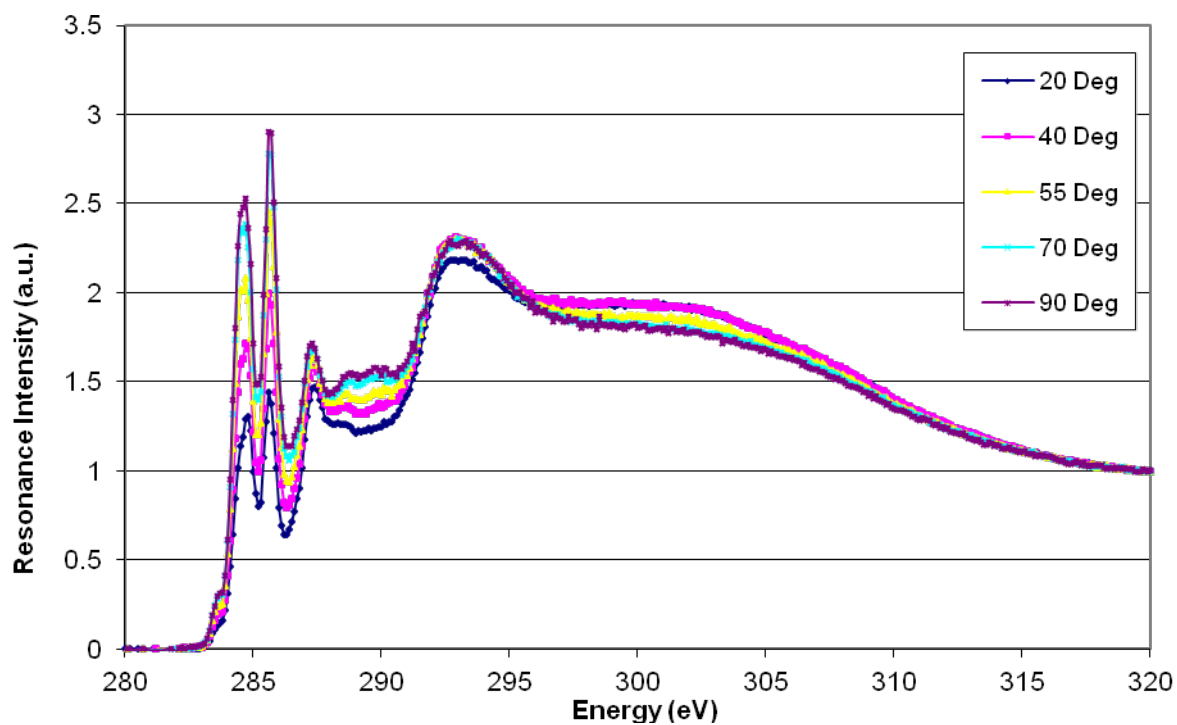
Fig. S14. Angle-resolved NEXAFS spectra for TMS-DBC **2b** at T_{sub} 55°C on SiO_2-ODTS surface.
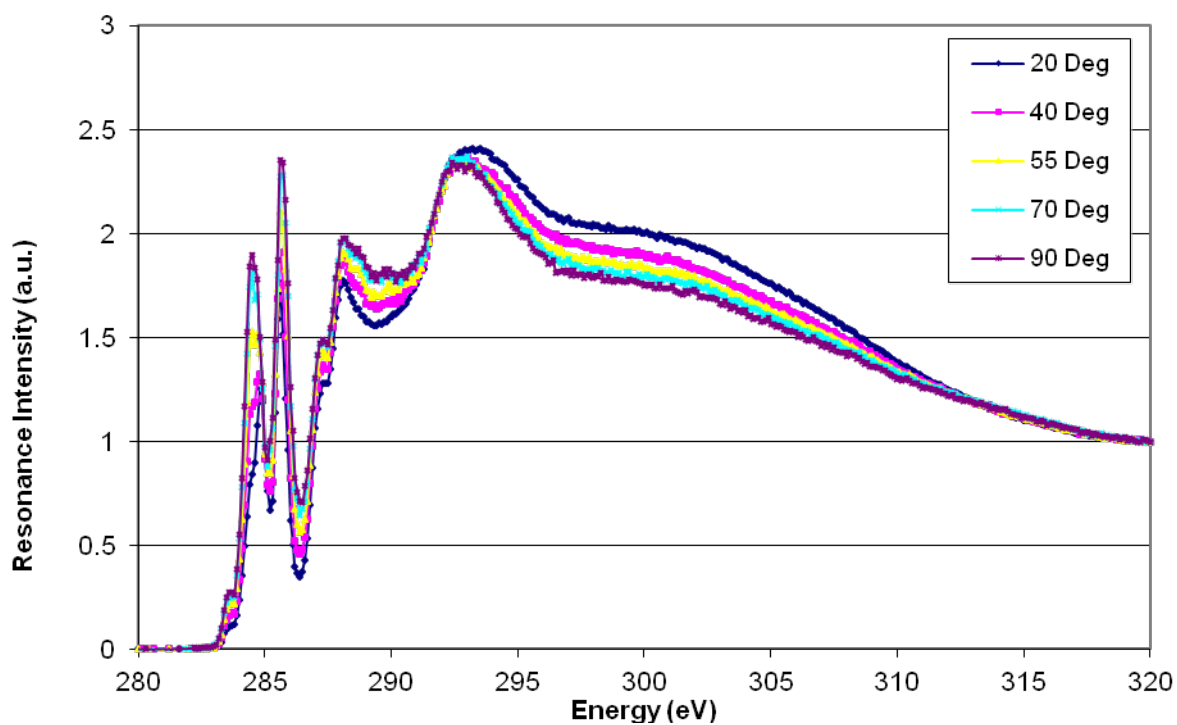

Fig. S15. Angle-resolved NEXAFS spectra for TIPS-DBC **2e** at T_{sub} 55°C on SiO_2-ODTS surface.

It is well known that the molecular orientation of films such as this can be found from the following equation;[4]

$$I \propto 1 - \tfrac{1}{2}(3\cos^2\theta - 1)(3\cos^2\alpha - 1)$$

where α is the average tilt angle related to the resonance peak in question and θ is the angle between the incident polarised light and the sample surface. Since the height of the relevant peaks in the π^* region of the NEXAFS spectra (~284-287eV) is proportional to the area; the average tilt angle of each film have been found by measuring the height of the π^* peak at 284.5 eV and fitting it to the equation above.

8.   Atomic Force Microscopy (AFM).

a) SiO_2, T_{sub} 25°C, RMS = 1 nm   b) SiO_2-HMDS, T_{sub} 25°C, RMS = 2 nm   c) SiO_2-ODTS , T_{sub} 25°C, RMS = ~23-24 nm

d) SiO_2, T_{sub} 55°C, RMS = 5 nm   e) SiO_2-HMDS, T_{sub} 55°C, RMS = 3 nm   f) SiO_2-ODTS , T_{sub} 55°C, RMS = 11 nm
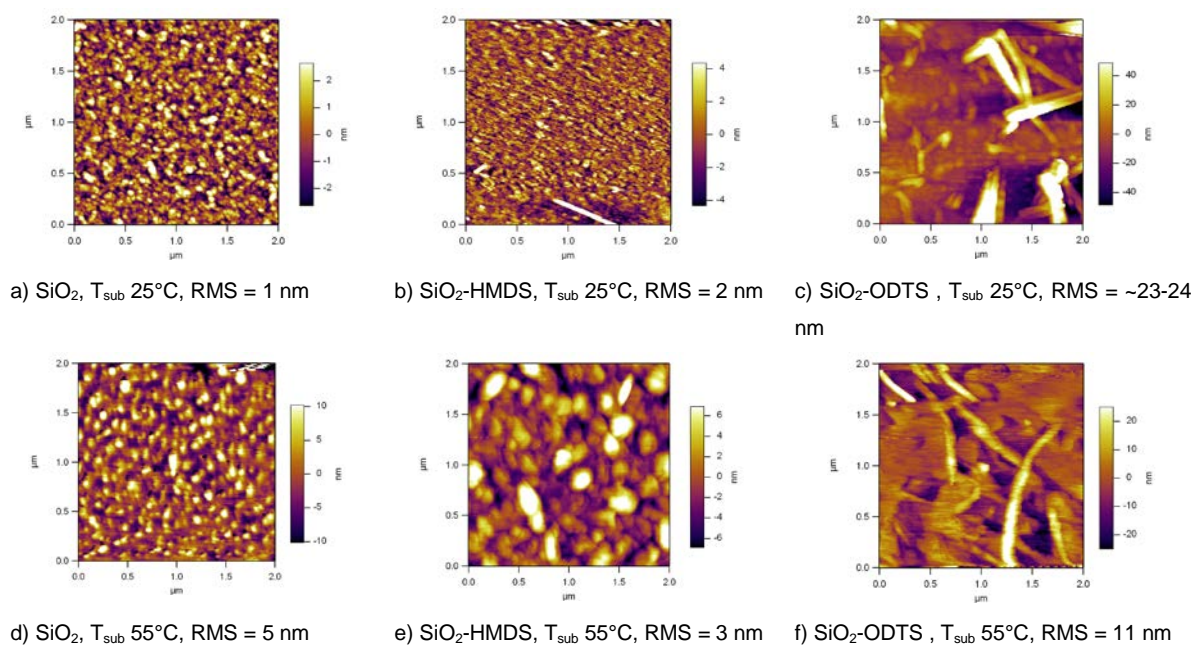
Fig. S16. AFM topography for TMS-DBC **2b** on different substrate surfaces and substrate temperatures.

18

9. References

1. M. J. Frisch, G. W. Trucks, H. B. Schlegel, G. E. Scuseria, M. A. Robb, J. R. Cheeseman, G. Scalmani, V. Barone, B. Mennucci, G. A. Petersson, H. Nakatsuji, M. Caricato, X. Li, H. P. Hratchian, A. F. Izmaylov, J. Bloino, G. Zheng, J. L. Sonnenberg, M. Hada, M. Ehara, K. Toyota, R. Fukuda, J. Hasegawa, M. Ishida, T. Nakajima, Y. Honda, O. Kitao, H. Nakai, T. Vreven, J. Montgomery, J. A., J. E. Peralta, F. Ogliaro, M. Bearpark, J. J. Heyd, E. Brothers, K. N. Kudin, V. N. Staroverov, T. Keith, R. Kobayashi, J. Normand, K. Raghavachari, A. Rendell, J. C. Burant, S. S. Iyengar, J. Tomasi, M. Cossi, N. Rega, J. M. Millam, M. Klene, J. E. Knox, J. B. Cross, V. Bakken, C. C. Adamo, J. Jaramillo, R. Gomperts, R. E. Stratmann, O. Yazyev, A. J. Austin, R. Cammi, C. Pomelli, J. W. Ochterski, R. L. Martin, K. Morokuma, V. G. Zakrzewski, G. A. Voth, P. Salvador, J. J. Dannenberg, S. Dapprich, A. D. Daniels, O. Farkas, J. B. Foresman, J. V. Ortiz, J. Cioslowski and D. J. Fox, Gaussian, Inc., Wallingford CT., 2010.
2. A.D. Becke, *J. Chem. Phys.*, 1993, **98**, 5648-5652.
3. K. B. Burke, Y. Shu, P. Kemppinen, B. Singh, M. Bown, I. Liaw, R. M. Williamson, L. Thomsen, P. Dastoor, W. Belcher, C. Forsyth, K. N. Winzenberg and G. E. Collis, *Cryst. Growth Des.*, 2012, **12**, 725−731.
4. J. Stöhr, *NEXAFS Spectroscopy*, Springer, Berlin, 1992.